Manganese distribution in the Mn-hyperaccumulator *Grevillea meisneri* from New Caledonia

Camille Bihanic
Laboratoire de Chimie Bio-inspirée et d'Innovations Écologiques, ChimEco
Eddy Petit
Institut Européen des Membranes, IEM – UMR 5635, ENSCM, CNRS – Université de Montpellier
Roseline Perrot
Service des Laboratoires Officiels Vétérinaires Agroalimentaires et Phytosanitaires de Nouvelle-Calédonie
Lucie Cases
Laboratoire de Chimie Bio-inspirée et d'Innovations Écologiques, ChimEco
Armelle Garcia
Laboratoire de Chimie Bio-inspirée et d'Innovations Écologiques, ChimEco
Franck Pelissier
Laboratoire de Chimie Bio-inspirée et d'Innovations Écologiques, ChimEco
Cyril Poullain
Laboratoire de Chimie Bio-inspirée et d'Innovations Écologiques, ChimEco
Camille Rivard
Synchrotron SOLEIL
Martine Hossaert
Laboratoire de Chimie Bio-inspirée et d'Innovations Écologiques, ChimEco
Claude Grison (claude.grison@cnrs.fr)
Laboratoire de Chimie Bio-inspirée et d'Innovations Écologiques, ChimEco https://orcid.org/0000-0002-2687-1520

Research Article

Keywords: Elemental mapping, Grevillea meisneri, Micro-X-Ray Fluorescence spectroscopy, Mn-hyperaccumulator, Mn distribution

Posted Date: April 12th, 2021

DOI: https://doi.org/10.21203/rs.3.rs-393514/v1

Version of Record: A version of this preprint was published at Scientific Reports on December 1st, 2021. See the published version at https://doi.org/10.1038/s41598-021-03151-9.

Abstract

• *Grevillea meisneri*, an endemic New Caledonian Mn-hyperaccumulator, is used in rehabilitation of degraded mining sites on the island. Large-scale programs require transplanting nursery-grown seedlings, but effects of the nursery environment on Mn tolerance of transplants and their capacity to hyper-accumulate Mn are unknown, slowing rehabilitation efforts.

• We studied tissue-level distribution of Mn and other elements in different tissues of *G. meisneri* using micro-X-Ray Fluorescence spectroscopy (μXRF), comparing nursery-grown plants transplanted into the site and sampled seven years later, and similar-sized plants that had grown spontaneously in the site.

• Mirroring patterns in other Mn-hyperaccumulators, Mn was preferentially accumulated in leaves but was also present in roots. Concentrations were highest in leaf epidermal tissues, in cortex and vascular tissues of stems and primary roots, and in phloem and pericycle-endodermis of parent cluster roots. Although abundant in soil, Ni was absent from all tissues of *G. meisneri*. Ca was always co-localised with Mn. Preferential uptake of Mn vs Ni in roots implies as-yet-uncharacterized specific Mn-transporters, while Ca and Mn co-localisation suggests shared transport pathways.

• No differences were observed in concentration and distribution of Mn in transplanted and spontaneously-growing plants. Nursery-grown transplants should be highly suitable for large-scale, high-throughput rehabilitation programs.

Introduction

Among the New Caledonian *Grevillea* species, *G. meisneri* Montrouz. (Proteaceae) is the only Manganese-hyperaccumulator, presenting up to 1% of Mn in shoots (Jaffré, 1977; Baker et al., 2000; Losfeld et al., 2015b). Restoration of vegetation cover on degraded mining sites is an urgent environmental concern in New Caledonia (Losfeld *et al.*, 2015a,b,c), and native pioneer species should be favoured in such actions. *Grevillea meisneri* was hence selected for a large-scale rehabilitation program. Mn-(hyper)accumulators are adapted to spontaneously grow on the ultramafic soils of New Caledonia, which are naturally poor in essential nutrients (e.g. P, Ca, K) but enriched in trace metallic elements such as Ni, Mn, Co, Cr and Sc (Jaffré, 1976; Gunkel-Grillon et al., 2014; Isnard et al., 2016). These plants exhibit the ability to accumulate Mn in their leaves at concentrations greatly exceeding those normal in other plants, as a response to the elevated concentrations of this metal in soils (Jaffré et al., 1977; Baker, 1981; Reeves, 2003; Pillon et al., 2010). The investigation of uptake and transportation mechanisms of the hyperaccumulated metal along with other physiological elements helps expand our knowledge of the phenomenon of hyperaccumulation.

While *G. meisneri* is known to be an Mn-hyperaccumulator, the distribution of Mn in its tissues has never been characterized in detail. One objective of our study was thus to describe and quantify the tissue distribution of Mn in this species. Micro-X-ray elemental mapping techniques give *in situ* information on the cellular distribution of elements within plant tissues, providing an effective immobilization of all their metabolic processes as close as possible to the native state of the sample. Using Synchrotron radiation

micro-X-Ray Fluorescence spectroscopy (mXRF), enabling mapping of Mn together with Ca, Cl, K, Mg, P and S, was conducted on cryo-fixed hydrated leaves, stem, roots and cluster roots of *G. meisneri*.

In efforts to rehabilitate sites polluted with heavy metals, the sites in which vegetation cover is to be restored are planted with large numbers of individuals of adapted species, usually ones native to, or even endemic to, soils naturally rich in these elements. However, the large number of individual trees required for these actions means that they must be grown *ex situ* as seedlings and then transplanted into the site that is slated for rehabilitation. An unanswered question is whether the environment experienced by the juveniles prior to transplantation affects their ability to adjust to the extreme conditions (including high concentrations of heavy metals) of the substrate *in situ*. Answering this question was another objective of this study. To this end, we compared the performance of individuals of *G. meisneri* growing spontaneously *in situ* in Mn-rich soils with that of individuals grown from seeds collected from conspecific adult trees in the same site that were sown in pots, grown in a nursery, and then transplanted into the rehabilitation site, where they grew for seven years before being sampled for this study. We compared their accumulation of Mn, and its tissue distribution, with those of plants that had grown *in situ* and were of comparable size. This enabled us to investigate the capacity of the reintroduced plants to adjust to the constraints of the ultramafic and contaminated soils.

Materials And Methods

Study species: Grevillea meisneri

This species is endemic to New Caledonia (Majourau & Pillon, 2020). It only grows on the northwestern coast of the 'Grande Terre', on 'maquis' of variable density, preferentially on brown hypermagnesian soils under 650 m altitude (Jaffré & Latham, 1974). Brown hypermagnesian soils are classified as Magnesic Cambisols (Fritsch, 2012). They are derived from ultramafic rocks, and are thus characterized by low concentrations of essential elements, particularly P, high concentrations of heavy metals such as Ni, Mn, Co, and Cr, and a high exchangeable Mg/Ca ratio (Isnard *et al*., 2016). *Grevillea meisneri,* being the only Mn-hyperaccumulator among the *Grevillea* species endemic to New Caledonia (Losfeld *et al*., 2015b) and being adapted to such edaphic conditions, was used to restore the degraded mining sites at 'Creek à Paul'. Use of transplanted plants in restoration efforts was considered a challenge. First, local environmental conditions –the high concentrations of metals in soil in addition to frequent water stress– make establishment difficult, even for species such as *G. meisneri* that are adapted to these conditions. Secondly, as noted above, it is not known whether juveniles grown in milder *ex situ* conditions are capable of adjusting, following transplantation, to the extreme conditions *in situ*, or whether they fully retain their capacity to tolerate, and to accumulate, Mn.

Plant materials

Restoration of the degraded mining site in 'Creek à Paul' valley near Tiébaghi (20°29'35.03"S, 164°12'22.76"E), New Caledonia, was carried out using plants of *G. meisneri*, among other (hyper)-accumulators of metals (e.g. Ni, Zn). In 2014, 450 plants of *G. meisneri* were obtained from seeds collected

in populations *in situ* and grown for 18 months in pots in a nursery, after which they were introduced into the mining site. Soil of each planting hole was prepared with Yates nutricote 365, Superphosphate triple and a water-retention agent. No further treatment was made post-plantation.

Harvesting of plant samples

Living plants of *G. meisneri* were collected from the 'Creek à Paul' valley in 2019. Harvests were made at the same time and respecting the legal authorizations of the North Province. Seven-year-old transplanted plants, and spontaneously growing specimens of the same height and living in the same valley, were selected (**Figure 1d**). Whole living plants were collected with their soil and were kept in pots for transportation to the laboratory, where samples were prepared within 24 h maximum post-harvest.

MP-AES analyses

Tissue samples including leaves, stems, roots and cluster roots of *G. meisneri* were carefully washed with deionized water to remove soil particles and then oven-dried at 60 °C overnight before being ground. Mineral composition was determined using an Agilent 4200 Microwave Plasma-Atomic Emission Spectrometer (MP-AES) coupled with an SPS4 autosampler. Approximatively 20 mg of the ground biomass was digested in 6 mL of reversed aqua regia (1:2 hydrochloric acid (37 %): nitric acid (65 %)) under an Anton Paar Multiwave Go microwave-assisted digestion, with the following program: 20 °C to 164 °C in 20 minutes then 10 minutes isothermal at 164 °C. Samples were filtered and then diluted to 0.2 g. L^{-1} in nitric acid (1 %). Three blanks were recorded for each step of the dilution procedure. Three analyses of the mineral composition were carried out for each sample to check repeatability of the measurement.

Ion chromatography

Ion chromatography analyses were carried out with a Metrohm 882 Compact IC instrument equipped with chemical (Metrohm suppressor MSM II for chemical) and sequential (Metrohm CO_2 suppressor MCS) suppression modules, and a conductivity detector. Separations were performed on a Metrosep A Supp 16 – 250/4.0 column associated with a guard column kept at 55 °C. The mobile phase consisted of a mixture of 7.5 mM Na_2CO_3 and 0.75 mM NaOH in ultrapure water. The flow rate was 0.8 mL min^{-1}. Standard solutions were prepared from a commercial multi-element standard solution of 1000 mg mL^{-1} of F^-, Cl^-, Br^-, NO_3^-, PO_4^- and SO_4^{2-} and from $Na_2C_2O_4$ and $C_4H_4O_5Na_2$. Analyses were carried out at Laboratoire de Chimie Physique et Microbiologie pour les Matériaux et l'Environnement (LCPME – Université de Lorraine, France). Two separate chromatography analyses were recorded for each sample.

The samples were prepared using fresh leaves that were ground in deionized water using a mortar and pestle. The homogenate was filtered and the filtrate was collected for analysis. The residue was then extracted with isopropanol in the same way. The resulting residue was then finally extracted with dichloromethane, following the same procedure. The three filtrates were collected and analyzed.

Light microscopy

Fresh samples of *G. meisneri*, including leaves, stems, roots and cluster roots were collected *in situ* and immediately fixed in formalin (10%) during 24 h. Fixed tissues were then embedded in paraffin (Paraplast plus) using a SAKURA VIP® 5 JR vacuum infiltration processor and a SAKURA TEC-5 embedding console. The samples were sectioned at 6 mm thickness under a rotary microtome (Leica RM2245). After staining with carmine red / iodine green, the tissue samples were examined using a light microscope (Leica DM3000) equipped with a camera (Leica MC170 HD).

Sample preparation for micro-XFM analyses

Leaves, stems, roots and cluster roots of living plants of *G. meisneri* were carefully washed with deionized water before being dried with absorbing paper. Samples were cut and fragments of about 1 cm long were immediately immersed in an embedding compound (Optimal Cutting Temperature OCT from VWR) and fast frozen in isopentane, as liquid cryogen, cooled by liquid nitrogen (Castillo-Michel *et al.*, 2017). This cryofixation protocol ensured an extremely fast cooling of the samples, preventing ice crystal formation. Therefore, it limited damage to the cellular structures and preserved elemental distribution close to its natural state. Leaf samples were divided into mid-rib (central vein) and margin. For the roots, the primary root and cluster roots were sampled. The samples were transported from New Caledonia in a cryogenic container, kept at -80 °C using dry ice, to SOLEIL Synchrotron (CEA Paris-Saclay) for analyses and kept in a freezer at -80 °C before cryo-sectioning.

Transverse sections of frozen-hydrated tissues were cut at a thickness of 20 µm using a cryo-microtome (Thermo Fisher Scientific). The cryo-chamber was kept at -20 °C. The thin sections were placed between two Ultralene films (SPEX SamplePrep) in a copper sample holder.

Synchrotron micro-X-ray Fluorescence Microscopy

The micro-X-ray fluorescence microscopy (µXRF) analyses were carried out at the LUCIA beamline (Vantelon *et al.*, 2016) at SOLEIL Synchrotron. The X-ray beam was monochromatized at 6.65 keV using a fixed exit double-crystal Si (111) monochromator. The beam was focused to 3.6 × 2.9 ($v \times h$) µm^2 by means of a Kirkpatrick-Baez mirrors arrangement. The XRF signal was collected using a mono-element (60 mm^2) Bruker silicon drift diode detector. Maps were collected in continuous Fly-scan mode with a pixel size of 3 × 3 µm^2 and an integration time of 200 ms per pixel for high spatial resolution maps. The selection of appropriate areas for high spatial resolution maps was based on low spatial resolution maps (pixel size between 10 × 10 and 100 x 100 µm^2 and with an integration time of 50 ms per pixel). Samples were scanned under cryogenic conditions using a liquid nitrogen cryostat, and under vacuum in order to limit absorption and scattering by air. Samples were transferred into the experimental chamber under liquid nitrogen vapor to maintain the cold chain.

Data processing and statistics

The count number for the XRF signal was normalized by the count number of the incoming beam signal and corrected by the XRF detector dead time. To optimize the discrimination of the various XRF line

contributions, the XRF signal of each element was extracted by batch fitting the XRF spectrum in each pixel of the map using the PyMCA software (Solé *et al.*, 2007).

Regions of interest (ROIs) were selected from the maps using the ROI tool in the Fiji software (Schindelin *et al.*, 2012) according to the tissues of the organs. The different types of tissues identified are reported in **Table 1**. Average fluorescence intensities of each element among the different tissues were obtained from the selected ROIs. Correlations between Mn, Ca, Cl, K, Mg, P and S concentrations were estimated by extracting fluorescence intensity pixel by pixel for each element from the selected ROIs. Unscramble (Camo analytics) was used to perform PCA analyses. Pearson correlation coefficients between the different elements and *P*-values were calculated using R (R Core Team). Holm's correction for multiple comparisons tests was applied.

Table 1. Tissues identified in the different organs of *Grevillea meisneri*. Tissues were collected from the outside to the inside of the corresponding organ.

Organ	Identified tissues
Leaf margin	Cuticle, upper epidermis, palisade mesophyll, spongy mesophyll, lower epidermis
Leaf mid-rib	Upper epidermis, palisade mesophyll, vascular bundles, spongy mesophyll, lower epidermis
Stem	Periderm, cortex, phloem, xylem, pith
Primary root	Periderm, cortex, phloem, xylem
Parent root and cluster rootlets	Cluster rootlets, epidermis, cortex, periderm and endoderm layers, phloem, xylem

Results

Morphology of Grevillea meisneri

Grevillea meisneri is a shrubby species that can reach up to 7 m height (**Figure 1a**). Its tortuous branches are glabrous, rubiginous when young, and the wood is ash grey. The leaves are simple, coriaceous, lanceolate to elliptic, 35-140 mm long x 6-70 mm wide, petiolate. The adaxial surface (hereinafter referred to as 'upper epidermis') is glabrous and shiny light-green whereas the abaxial surface (hereinafter referred to as 'lower epidermis') is hairy, matte and brownish, even silver-grey. The entire margin is entirely recurved underneath and the fine pinnate venation is barely visible. The brightly coloured carmine-red flowers are clustered into simple, cylindrical and pendulous racemes at the end of branches (**Figure 1b**) (L'Huillier *et al.*, 2010). Like other Proteaceae, *Grevillea meisneri* is non-mycorrhizal but, like almost all other members of the family, develops cluster roots to improve nutrient uptake (**Figure 1c**) (Purnell, 1960; Dinkelaker *et al.*, 1995; Lamont, 2003; Shane & Lambers, 2005). The morphology of plants that had been transplanted and those that had grown spontaneously in the rehabilitation site was similar; no visual differences could be established to differentiate them.

Bulk elemental composition in plant tissues of Grevillea meisneri

The elemental composition of tissues of *G. meisneri* was analysed by MP-AES (**Table 2**). Calcium was the major mineral element in all plant tissues analysed, with a range of concentrations of 0.5 – 0.8 wt % (DW). Manganese presented concentrations similar to or even higher than those of macronutrient elements such as Ca, K and Mg in each tissue and especially in leaves, with up to 0.4 wt %. This was not surprising, as *G. meisneri* is a Mn-hyperaccumulating species. Even higher concentrations of Mn could have been expected in leaves, as a mean concentration of 0.7 wt % (and a maximum of 1.1 wt %) was previously found in leaves of *G. meisneri* (Losfeld *et al.*, 2015b). However, the lower values for Mn concentrations obtained in this study using young leaves could be explained by the previously established relationship between leaf age and foliar concentration of Mn, with the oldest leaves having the highest Mn concentrations. Mirroring the results for leaf morphology, no significant differences in concentrations of Mn were observed between plants that had been transplanted and those that had grown spontaneously in the rehabilitation site. Since *G. meisneri* in this site grows on soil enriched in Ni, the abundance of this element was measured as well, but its presence was not detected in any part of the plant.

Concentrations of P and S in leaves were determined by ICP-MS (**Table S1**). The concentration of P was very low, even lower than the concentration of S, as in other native New Caledonian species of the genus. Conversely, the cultivated variety known as "*Grevillea rosa jenkinsii"*, derived from the Australian species *Grevillea rosmarinifolia* A. Cunn., presented a much higher P concentration (**Table S1**).

Table 2. Elemental composition in tissues of plants of *Grevillea meisneri* that had been transplanted (T) and plants that had grown spontaneously (S) in the rehabilitation site, determined by MP-AES analyses.

Tissues	Group	Composition (wt % (± S.E.))				
		Mn	Ca	K	Mg	Na
Leaves	T (7)	0.31 (± 0.09)	0.59 (± 0.07)	0.30 (± 0.07)	0.23 (± 0.06)	0.12 (± 0.03)
	S (8)	0.39 (± 0.21)	0.55 (± 0.16)	0.29 (± 0.11)	0.11 (± 0.04)	0.18 (± 0.10)
Stems	T (4)	0.14 (± 0.05)	0.63(± 0.19)	0.35 (± 0.12)	0.13 (± 0.06)	0.09 (± 0.04)
	S (2)	0.22 (± 0.08)	0.50 (± 0.04)	0.10 (± 0.08)	0.17 (± 0.04)	0.15 (±0.02)
Primary roots	T (6)	0.06 (± 0.03)	0.24 (± 0.08)	0.11 (± 0.09)	0.14 (± 0.04)	0.08 (± 0.02)
	S (6)	0.20 (± 0.10)	0.74 (± 0.25)	0.20 (± 0.11)	0.23 (± 0.20)	0.16 (± 0.06)
Parent cluster roots	T (6)	0.12 (± 0.03)	1.00 (± 0.28)	0.31 (± 0.18)	0.29 (± 0.06)	0.43 (± 0.09)
	S (2)	0.21 (± 0.11)	0.49 (± 0.02)	0.11 (± 0.08)	0.44 (± 0.36)	0.22(± 0.01)

Numbers in brackets denote the separate samples analysed. Ni was also analysed but not detected.

Ion chromatography of Grevillea meisneri *leaves*

Chemical composition of the leaves of *G. meisneri* was further analyzed by ion chromatography. The presence of carboxylates was investigated and analyses revealed a high content in malate and oxalate, while citrate could not be detected. Two other anions were abundant, sulfate and phosphate, accompanied by concentrations of PO_4^{3-} about four times higher, which is surprising for a plant belonging to the family Proteaceae, which can grow on soil depleted in phosphorus, such as the serpentine soils of New Caledonia.

Table 3. Concentrations of anions in leaves of *Grevillea meisneri,* determined by ion chromatography analyses.

Concentration ($mg.L^{-1}$)				
[malate]	[oxalate]	[citrate]	$[SO_4^{2-}]$	$[PO_4^{3-}]$
14.6	7.7	nd	10.9	39.2

Anatomical features of Grevillea meisneri *leaves, stems and roots*

Light microscopic analysis was conducted on leaves, stems and roots of *G. meisneri*. Mirroring results from the analyses presented above, no differences were observed in anatomical features of plants that had been transplanted and those that had grown spontaneously in the rehabilitation site.

Light microscopy images of leaves showed a thick cuticular layer, as expected for a xerophytic species (**Figure 2a, b**). The upper epidermis is composed of a single layer of large cells, twice as large as those of the lower epidermis. The palisade mesophyll consists of thin, elongated cells aligned in a single layer, as was observed using PIXE/EDS and SEM/EDS for *Grevillea exul* (Fernando *et al*., 2008a). The spongy mesophyll took up more than half of the total thickness of the mesophyll. The dermal layers accounted for about 25% of the total leaf volume.

The stems exhibited a typical secondary growth structure with a small cortex, a large stele with well-defined vascular bundles and a periderm, which comprises the outermost tissue of the stem (**Figure 2c**). Likewise, the primary roots had a typical secondary growth root structure (**Figure 2d**). Samples of cluster roots were cut so as to obtain a cross section of the parent root, so only a tangential section of cluster rootlets stemming from the parent root could be mapped (**Figure 2e**). Light microscopy images of cluster roots clearly revealed the primary structure of the parent root, with a wide parenchymatous cortex split by cluster rootlets. The rootlets seemed to emerge from the parental pericycle, opposite the xylem poles, as first described by Purnell (1960) for the general structure of cluster roots. The tangential section of the cluster rootlets could not give much information concerning the anatomical structure of the rootlets.

Elemental distribution in leaves, stems and roots of Grevillea meisneri *determined by micro-XRF*

Micro-X-ray fluorescence was performed on leaves, stems, roots and cluster roots of transplanted and spontaneously growing plants of *G. meisneri* and provided elemental mapping of frozen hydrated tissues as close as possible to the native state (Fernando *et al*., 2013). The mXRF maps of *G. meisneri* leaves,

stems and roots showed no differences in elemental distributions between the two groups of plants. The brightness of each mXRF map was scaled for an optimum contrast, so the pixel intensities did not represent relative differences in concentration between elements, but represented differences in concentration for a single element. Micro-XRF maps of K were used as a control since the presence of cellular K in all samples indicated the retention of cell content, thus showing the efficiency of the preparation.

Micro-XRF maps of the leaves revealed that Mn was sequestered in the epidermis, mostly in the lower epidermis, and was found, in lower concentrations, in vascular tissues and the spongy mesophyll (**Figure 3** and **Figure S1, S2**). Ca was also mostly localized in the dermal layers, with a higher concentration in the upper epidermis. High-intensity Ca spots throughout the spongy mesophyll suggested the presence of calcium oxalate crystals. Magnesium was mostly localized in the dermal tissues. Other nutrient elements (K, Cl, S and P) were globally distributed throughout the leaves. However, P showed a higher concentration in the vascular tissues whereas S was mostly in the mesophyll (**Figure S2**).

Micro-XRF maps of the stem showed that Mn was highly concentrated in the cortex, sixfold higher than in other parts of the stem, and was also found in the vascular tissues, particularly in the phloem (**Figure 4** and **Figure S3**). Ca was also localized in the cortex and highly concentrated in cells aligned in axial rays around the xylem, which constituted a Ca enrichment in medullary rays, a finding previously reported in the Ni-hyperaccumulator *Rinorea* cf. *javanica* (van der Ent *et al.*, 2020). A similar distribution was observed for S and Mg. Potassium was homogeneously distributed through the stem, with a slightly higher concentration in the phloem, whereas P attained its highest concentrations in the xylem. Chlorine was mostly in the cortex as well as in the inner periderm.

Micro-XRF maps of the primary roots showed that Mn was mainly localised in the cortex and the phloem, the cortex showing the highest Mn concentration (**Figure 5** and **Figure S4**). In the cortex, Mn was mostly localized in the apoplastic spaces. Similarly to Mn, Ca was located in the cortex and in the phloem, but with the highest concentration in the latter tissue. C was concentrated in the phloem and inner periderm. K distribution mirrored that of Cl with a strong enrichment in the phloem. P was concentrated in the vascular tissues of the roots.

Micro-XRF maps of the cluster roots showed that Mn was mainly concentrated in the phloem and in the pericycle-endodermis layers of the parent cluster root (**Figure 6** and **Figure S5**, **S6**). To a lesser extent, Mn was distributed in the cortex. Ca was distributed throughout the parent cluster root and the rootlet, principally in the pericycle-endodermis layers and phloem. Cl was concentrated in the cortex in the parent cluster roots, and K, Mg and S were evenly distributed throughout the parent cluster roots, with a minor enrichment in the phloem. P was mainly localized in the phloem of the parent cluster roots.

PCA analyses and correlations

PCA analyses were performed for each element on every tissue of the different organs of *G. meisneri* to investigate co-localisation of the elements, with a particular focus on Mn (**Table 4 and Fig S7**), since it is

the hyperaccumulated element.

Data used for PCA analyses were collected from the tissues of each organ in which Mn was the most highly concentrated, i.e., the dermal layers for the leaf, the cortex for the stem, the cortex of the primary root, and the pericycle-endodermis layers and phloem of the parent cluster root. Interestingly, in each organ a strong positive correlation between Mn and Ca concentrations was observed ($P \leq 0.0001$). Overall, no other such strong positive correlations were found between Mn and another physiological element, except for Mn/Mg correlation in the upper epidermis of the leaf and in the cortex of the stem, as well as positive Mn/K and Mn/Cl correlations in the phloem of the parent cluster root.

Table 4. Pearson correlation coefficients between Mn and other physiological elements among the main Mn sinks of the different organs of Grevillea. meisneri (ue: upper epidermis; le: lower epidermis; c: cortex; pe-en: pericycle-endodermis layers; p: phloem). P-values are all ≤ 0.0001, except where indicated. Values of Pearson correlation coefficient higher than 0.5 are indicated in bold characters.

Organ	Tissue	Mn/Ca	Mn/Cl	Mn/K	Mn/Mg	Mn/P	Mn/S
Leaf margin	ue	**0.68**	**0.53**	0.40	0.47	0.40	**0.51**
	le	**0.94**	0.48	0.45	0.30	0.43	0.44
Leaf mid-rib	ue	**0.98**	0.28	0.45	**0.73**	0.39	0.45
	le	**0.73**	0.23	0.27	0.36	0.32	0.30
Stem	c	**0.60**	0.11	0.34	**0.56**	0.47	0.41
Primary root	c	**0.89**	0.48	0.38	0.28	0.26	0.12
Parent cluster Root	pe-en	**0.84**	0.43	0.49	0.45	0.46	0.45
	p	**0.94**	**0.72**	**0.73**	0.25	-0.11[#]	0.04 [# #]

[#] *P*-value: 0.0007

[# #] *P*-value: 0.17

Discussion

Many studies using microbeam technologies have reported the elemental composition in leaves and stems of (hyper)accumulators growing spontaneously on Mn-enriched sites. Here, studying *G. meisneri*, a Mn-hyperaccumulator of New Caledonia, we compared elemental composition in leaves, stems, roots, and cluster roots of two groups of plants: plants that had grown spontaneously on the rehabilitation site, and nursery-grown plants, grown from seeds taken from adults in the same site that had been transplanted into the site and allowed to grow for seven years. No differences in morphology, anatomy, or elemental concentration and distribution, particularly of Mn, were observed between the two groups. These results

suggest that the pre-transplant environment experienced by the transplanted group had no effect on their ability to tolerate, assimilate and accumulate Mn.

The global distribution of Mn in *G. meisneri* presented the highest concentration of Mn in leaves, as expected for a (hyper)accumulated metal, but substantial concentrations of Mn were also found in roots. Interestingly, no Ni was detected in any part of the plant, although *G. meisneri* grew on Ni-enriched soil and was surrounded by Ni-hyperaccumulator species. Specific transporters of Mn^{2+}, such as carboxylate complexes that are secreted by cluster roots of Proteaceae (Neumann & Martinoia, 2002), might explain this specific uptake mechanism towards Mn versus Ni. In several Mn-(hyper)accumulators, including *G. exul*, citrate and malate were found to be the most plausible counter-ions associated with Mn(II) (Fernando *et al.*, 2010). Ion chromatography analyses of leaves of *G. meisneri* revealed high contents of malate and oxalate while citrate could not be detected. This suggests that malate and/or oxalate could be involved in the sequestration of Mn in leaves of *G. meisneri*.

In leaves of *G. meisneri*, Mn was mainly sequestered in the epidermal tissues. The foliar sequestration of metals, including Mn (Fernando *et al.*, 2008b, Fernando *et al.*, 2008a, Memon *et al.*, 1980, 1981, Xu *et al.*, 2006), Ni (Krämer *et al.*, 1997; Mesjasz-Przybyłowicz *et al.*, 2001; Küpper *et al.*, 2001; Robinson *et al.*, 2003; Bidwell *et al.*, 2004), Zn, and Cd (Vázquez *et al.*, 1992; Küpper *et al.*, 2000), usually occurs in non-photosynthetic tissues, enabling avoidance of any damage to cell metabolic activities. Here, the symmetrical accumulation of Mn in epidermal layers might act as a chemical defence strategy against herbivory. In favour of this hypothesis is the observation that the lower epidermis presented more enrichment in Mn than the upper one, similar to findings for other heavy metals in other accumulator plants (Boyd & Martens, 1992; Küpper *et al.*, 2000, 2001; Krämer *et al.*, 2000; Asemaneh *et al.*, 2006). Many insect herbivores prefer to feed on leaf undersides, where the cuticle is often less tough, and where the insects have a little bit of shade. Although Mn is considered less toxic to plants than other metals, its detoxification is needed for Mn-hyperaccumulators and their strategy relies on cell vacuolation for Mn sequestration in leaves (Küpper *et al.*, 1999, 2000; Fernando *et al.*, 2012). Although the resolution of mXRF was not sufficient to discern subcellular elemental localizations, the shape of Mn distribution in the epidermal layers, and the wide vacuolar volumes of the large dermal cells compared to the thin cells of the palisade, strongly suggest a vacuolar sequestration, without excluding localization in cell walls.

In the stem, the presence of Mn in the vascular tissues and in the cortex could be respectively explained by its transportation from root to shoot and from shoot to older leaves (Shao *et al.*, 2017), and by its sequestration. Both mechanisms could represent an adaptive strategy developed by *G. meisneri* facing excessive concentrations of Mn.

Mn distribution in the primary roots revealed the early uptake of Mn through the apoplastic pathway in the cortex, before entering the symplast in the endoderm, then reaching the phloem, but not the xylem. Similar distribution of Mn has also been observed in the roots of *Gossia fragrantissima* (Myrtaceae) (Abubakari *et al.*, 2021). Further investigations are needed to deepen our understanding of Mn transportation, considering its low mobility in the phloem sap (White, 2012) and its transportation from root to shoot in the xylem (Marschner, 2012).

Strong positive Mn/Ca correlations were observed in every tissue of *G. meisneri* where Mn was the most concentrated. Such positive Mn/Ca correlations has also been found in the dermal layers of other Mn-hyperaccumulators, *Garcinia amplexicaulis* (Clusiaceae) (Fernando *et al.*, 2012), *Gossia grayi* and *G. shepherdii* (Myrtaceae) (Fernando *et al.*, 2018). Mn(II) is the predominant ionic form of Mn in plants and shares similar radius and chemical features (hardness according to HSAB theory) with Ca(II) (Pearson, 1968). Although this similarity could lead to competitive ionic antagonism (Marschner, 2012) and explain a negative Mn/Ca correlation observed in the main Mn sequestration sites of two *Gossia* species (Fernando *et al.*, 2018), this similarity could explain, in our study, the positive Mn/Ca correlation via a cooperative uptake and transportation pathway in *G. meisneri* (Alejandro *et al.*, 2020). Indeed, many transporters of Ca(II), such as some membrane Ca^{2+} channels, are reported to permeate Mn in *Arabidopsis thaliana* (Brassicaceae) and in *Acanthopanax sciadophylloides* (Araliaceae) (Hirschi *et al.*, 2000; Wu *et al.*, 2002; Pittman, 2005; Mills *et al.*, 2008; Mizuno *et al.*, 2013).

Using nursery-grown plants could supply the large numbers of plants required if rehabilitation efforts are to be attempted at the massive scales needed for a truly significant environmental impact. However, workers have been reluctant to use nursery-grown plants because of uncertainty about their capacity to adjust, following transplantation, to the harsh environments of the rehabilitation sites. We found that plants grown *ex situ* from seeds of adult *G. meisneri* trees growing in Mn-rich soils and then transplanted into the rehabilitation site had the same capacity to tolerate, assimilate and hyper-accumulate Mn as plants that had grown spontaneously in the site. A potential objection to the use of nursery-grown plants in rehabilitation efforts is thus removed, further suggesting the feasibility of actions on larger scales than have previously been attempted.

Declarations

Acknowledgments

We acknowledge CNRS and SOLEIL for provision of synchrotron radiation facilities. We also thank SLN for our collaboration and Northern Province of New Caledonia for harvest authorizations (609011-40/2019/DEPART/JJC). Finally, Sci-GuidEdit company is acknowledged for writing assistance and proofreading the article.

Author contributions

C.G. and C.R. conceived and designed the study. C.B., A.G., C. P. , R.P. and L.C. carried out the harvest, preparation of samples and analyses. M.H., C.G., C.B. and E.P. completed integrated data analyses and wrote the paper.

Bibliography

Abubakari F, Nkrumah PN, Fernando DR, Brown GK, Erskine PD, Echevarria G, van der Ent A. 2021. Incidence of hyperaccumulation and tissue-level distribution of manganese, cobalt and zinc in the genus

Gossia (Myrtaceae). *Metallomics* doi.org/10.1093/mtomcs/mfab008

Alejandro S, Höller S, Meier B, Peiter E. 2020. Manganese in plants: from acquisition to subcellular allocation. *Frontiers in Plant Science* **11**: 300.

Asemaneh T, Ghaderian SM, Crawford SA, Marshall AT, Baker AJM. 2006. Cellular and subcellular compartmentation of Ni in the Eurasian serpentine plants *Alyssum bracteatum, Alyssum murale* (Brassicaceae) and *Cleome heratensis* (Capparaceae). *Planta* **225**: 193–202.

Baker AJM. 1981. Accumulators and excluders -strategies in the response of plants to heavy metals. *Journal of Plant Nutrition* **3**: 643–654.

Baker AJM, McGrath SP, Reeves RD, Smith JAC. 2000. Metal hyperaccumulator plants: a review of the ecology and physiology of a biological resource for phytoremediation of metal-polluted soils. In:Terry N, Bañuelos G, eds. *Phytoremediation of contaminated soil and water*. Lewis Publishers, Boca Raton, FL: 85–107.

Bidwell SD, Crawford SA, Woodrow IE, Sommer-Knudsen J, Marshall AT. 2004. Sub-cellular localization of Ni in the hyperaccumulator, *Hybanthus floribundus* (Lindley) F. Muell. *Plant, Cell & Environment* **27**: 705–716.

Boyd RS, Martens SN. 1992. The raison d'etre for metal hyperaccumulation by plants. In: Baker AJM, Proctor J, Reeves RD, eds. *The vegetation of ultramafic (serpentine) soils.* Andover, Hampshire, England: Intercept, 279–289.

Dinkelaker B, Hengeler C, Marschner H. 1995. Distribution and function of proteoid roots and other root clusters. *Botanica Acta* **108**: 183–200.

van der Ent A, de Jonge MD, Mak R, Mesjasz-Przybyłowicz J, Przybyłowicz WJ, Barnabas AD, Harris HH. 2020. X-ray fluorescence elemental mapping of roots, stems and leaves of the nickel hyperaccumulators *Rinorea* cf. *bengalensis* and *Rinorea* cf. *javanica* (Violaceae) from Sabah (Malaysia), Borneo. *Plant and Soil* **448**:15–36.

Fernando DR, Marshall A, Baker AJM, Mizuno T. 2013. Microbeam methodologies as powerful tools in manganese hyperaccumulation research: present status and future directions. *Frontiers in Plant Science* **4**: 319.

Fernando DR, Marshall AT, Gouget B, Carrière M, Collins RN, Woodrow IE, Baker AJ. 2008a. Novel pattern of foliar metal distribution in a manganese hyperaccumulator. *Functional Plant Biology* **35**: 193-200.

Fernando DR, Marshall AT, Green PT. 2018. Cellular ion interactions in two endemic tropical rainforest species of a novel metallophytic tree genus. *Tree Physiology* **38**: 119–128.

Fernando DR, Mizuno T, Woodrow IE, Baker AJM, Collins RN. 2010. Characterization of foliar manganese (Mn) in Mn (hyper)accumulators using X-ray absorption spectroscopy. *The New Phytologist* **188**: 1014–1027.

Fernando DR, Woodrow IE, Baker AJM, Marshall AT. 2012. Plant homeostasis of foliar manganese sinks: specific variation in hyperaccumulators. *Planta* **236**: 1459–1470.

Fernando DR, Woodrow IE, Jaffré T, Dumontet V, Marshall AT, Baker AJM. 2008b. Foliar manganese accumulation by *Maytenus founieri* (Celastraceae) in its native New Caledonian habitats: populational variation and localization by X-ray microanalysis. *New Phytologist* **177**: 178–185.

Fritsch E. 2012. Les sols. In: Bonvallot J, Gay J-C, Habert E, eds. *Atlas de la Nouvelle Calédonie.* Marseille: IRD, 73–76.

Gunkel-Grillon P, Laporte-Magoni C, Lemestre M, Bazire N. 2014. Toxic chromium release from nickel mining sediments in surface waters, New Caledonia. *Environmental Chemistry Letters* **12**: 511–516.

Hirschi KD, Korenkov VD, Wilganowski NL, Wagner GJ. 2000. Expression of *Arabidopsis* CAX2 in Tobacco. Altered Metal Accumulation and Increased Manganese Tolerance. *Plant Physiology* **124**: 125–134.

Isnard S, L'huillier L, Rigault F, Jaffré T. 2016. How did the ultramafic soils shape the flora of the New Caledonian hotspot? *Plant and Soil* **403**: 53–76.

Jaffré T. 1976. Composition chimique et conditions de l'alimentation minérale des plantes sur roches ultrabasiques (Nouvelle Calédonie). *Cahiers ORSTOM, Sér. Biol.*, **XI**: 53-63.

Jaffré T. 1977. Accumulation du manganèse par des espèces associées aux terrains ultrabasiques de Nouvelle Calédonie. *Comptes Rendus de l'Académie des Sciences.Série D: Sciences Naturelles* **284**: 1573–1575.

Jaffré T, Latham M. 1974. Contribution à l'étude des relations sol-végétation sur un massif de roches ultrabasiques de la côte Ouest de la Nouvelle Calédonie: le Boulinda. *Adansonia. Série 2* **14**: 311–336.

Jaffré T, Latham M, Schmid M. 1977. Aspects de l'influence de l'extraction du minerai de nickel sur la végétation et les sols en Nouvelle-Calédonie. *Cahiers ORSTOM. Série Biologie: Ecologie et Biologie Végétale* **12**: 307–321.

Krämer U, Grime GW, Smith JAC, Hawes CR, Baker AJM. 1997. Micro-PIXE as a technique for studying nickel localization in leaves of the hyperaccumulator plant *Alyssum lesbiacum. Nuclear Instruments and Methods in Physics Research Section B: Beam Interactions with Materials and Atoms* **130**: 346–350.

Krämer U, Pickering IJ, Prince RC, Raskin I, Salt DE. 2000. Subcellular localization and speciation of nickel in hyperaccumulator and non-accumulator *Thlaspi* species. *Plant Physiology* **122**: 1343–1353.

Küpper H, Jie Zhao F, McGrath SP. **1999**. Cellular compartmentation of zinc in leaves of the hyperaccumulator *Thlaspi caerulescens*. *Plant Physiology* **119**: 305–312.

Küpper H, Lombi E, Zhao F-J, McGrath SP. **2000**. Cellular compartmentation of cadmium and zinc in relation to other elements in the hyperaccumulator *Arabidopsis halleri*. *Planta* **212**: 75–84.

Küpper H, Lombi E, Zhao F-J, Wieshammer G, McGrath SP. **2001**. Cellular compartmentation of nickel in the hyperaccumulators *Alyssum lesbiacum, Alyssum bertolonii* and *Thlaspi goesingense*. *Journal of Experimental Botany* **52**: 2291–2300.

Lamont BB. **2003**. Structure, ecology and physiology of root clusters – a review. *Plant and Soil* **248**: 1–19.

L'Huillier L, Jaffre T, Wulff A, Lebrun M, Maggia L, Barre N, Chazeau J, Jourdan H, Amir H, Ducousso M, *et al.* 2010. *Mines et environnement en Nouvelle-Caledonie : les milieux sur substrats ultramafiques et leur restauration*. Paita: Ed. IAC.

Losfeld G, L'Huillier L, Fogliani B, Jaffré T, Grison C. **2015a**. Mining in New Caledonia: environmental stakes and restoration opportunities. *Environmental Science and Pollution Research* **22**: 5592–5607.

Losfeld G, L'Huillier L, Fogliani B, Mc Coy S, Grison C, Jaffré T. **2015b**. Leaf-age and soil-plant relationships: key factors for reporting trace-elements hyperaccumulation by plants and design applications. *Environmental Science and Pollution Research International* **22**: 5620–5632.

Losfeld G, Mathieu R, L'Huillier L, Fogliani B, Jaffré T, Grison C. **2015c**. Phytoextraction from mine spoils: insights from New Caledonia. *Environmental Science and Pollution Research* **22**: 5608–5619.

Majourau P, Pillon Y. **2020**. A review of *Grevillea* (Proteaceae) from New Caledonia with the description of two new species. *Phytotaxa* **477**: 243–252.

Marschner H. **2012**. *Marschner's Mineral Nutrition of Higher Plants* (P Marschner, Ed.). Academic Press.

Memon AR, Chino M, Hara K, Yatazawa M. **1981**. Microdistribution of manganese in the leaf tissues of different plant species as revealed by X-ray microanalyzer. *Physiologia Plantarum* **53**: 225–232.

Memon AR, Chino M, Takeoka Y, Hara K, Yatazawa M. **1980**. Distribution of manganese in leaf tissues of manganese accumulator: *Acanthopanax sciadophylloides* as revealed by Electronprobe X-Ray Microanalyzer. *Journal of Plant Nutrition* **2**: 457–476.

Mesjasz-Przybyłowicz J, Przybyłowicz W, Pineda C. **2001**. Nuclear microprobe studies of elemental distribution in apical leaves of the Ni hyperaccumulator *Berkheya coddii*. *South African Journal of Science* **97**: 591-593.

Mills RF, Doherty ML, López-Marqués RL, Weimar T, Dupree P, Palmgren MG, Pittman JK, Williams LE. **2008**. ECA3, a Golgi-Localized P2A-Type ATPase, Plays a crucial role in manganese nutrition in *Arabidopsis*. *Plant Physiology* **146**: 116–128.

Neumann G, Martinoia E. 2002. Cluster roots – an underground adaptation for survival in extreme environments. *Trends in Plant Science* **7**: 162–167.

Pearson RG. 1968. Hard and soft acids and bases, HSAB, part 1: Fundamental principles. *Journal of Chemical Education* **45**: 581.

Pillon Y, Munzinger J, Amir H, Lebrun M. 2010. Ultramafic soils and species sorting in the flora of New Caledonia. *Journal of Ecology* **98**: 1108–1116.

Pittman JK. 2005. Managing the manganese: molecular mechanisms of manganese transport and homeostasis. *The New Phytologist* **167**: 733–742.

Purnell HM. 1960. Studies of the family Proteaceae. I. Anatomy and morphology of the roots of some Victorian species. *Australian Journal of Botany* **8**: 38–50.

Reeves RD. 2003. Tropical hyperaccumulators of metals and their potential for phytoextraction. *Plant and Soil* **249**: 57–65.

Robinson BH, Lombi E, Zhao FJ, McGrath SP. 2003. Uptake and distribution of nickel and other metals in the hyperaccumulator *Berkheya coddi*i. *New Phytologist* **158**: 279–285.

Schindelin J, Arganda-Carreras I, Frise E, Kaynig V, Longair M, Pietzsch T, Preibisch S, Rueden C, Saalfeld S, Schmid B, *et al.* 2012. Fiji: an open-source platform for biological-image analysis. *Nature Methods* **9**: 676–682.

Shane MW, Lambers H. 2005. Manganese accumulation in leaves of *Hakea prostrata* (Proteaceae) and the significance of cluster roots for micronutrient uptake as dependent on phosphorus supply. *Physiologia Plantarum* **124**: 441–450.

Shao JF, Yamaji N, Shen RF, Ma JF. 2017. The Key to Mn homeostasis in plants: Regulation of Mn transporters. *Trends in Plant Science* **22**: 215–224.

Solé VA, Papillon E, Cotte M, Walter Ph, Susini J. 2007. A multiplatform code for the analysis of energy-dispersive X-ray fluorescence spectra. *Spectrochimica Acta Part B: Atomic Spectroscopy* **62**: 63–68.

Vantelon D, Trcera N, Roy D, Moreno T, Mailly D, Guilet S, Metchalkov E, Delmotte F, Lassalle B, Lagarde P, *et al.* 2016. The LUCIA beamline at SOLEIL. *Journal of Synchrotron Radiation* **23**: 635–640.

Vázquez MD, Barceló J, Poschenrieder Ch, Mádico J, Hatton P, Baker AJM, Cope GH. 1992. Localization of zinc and cadmium in *Thlaspi caerulescens* (Brassicaceae), a metallophyte that can hyperaccumulate both metals. *Journal of Plant Physiology* **140**: 350–355.

White PJ. 2012. Chapter 3 - Long-distance Transport in the Xylem and Phloem. In: Marschner P, ed. Marschner's *Mineral Nutrition of Higher Plants*, 3rd Edition. San Diego: Academic Press, 49–70.

Wu Z, Liang F, Hong B, Young JC, Sussman MR, Harper JF, Sze H. 2002. An endoplasmic reticulum-bound Ca(2+)/Mn(2+) pump, ECA1, supports plant growth and confers tolerance to Mn(2+) stress. *Plant Physiology* **130**: 128–137.

Xu X, Shi J, Chen Y, Chen X, Wang H, Perera A. 2006. Distribution and mobility of manganese in the hyperaccumulator plant *Phytolacca acinosa* Roxb. (Phytolaccaceae). *Plant and Soil* **285**: 323–331.

Figures

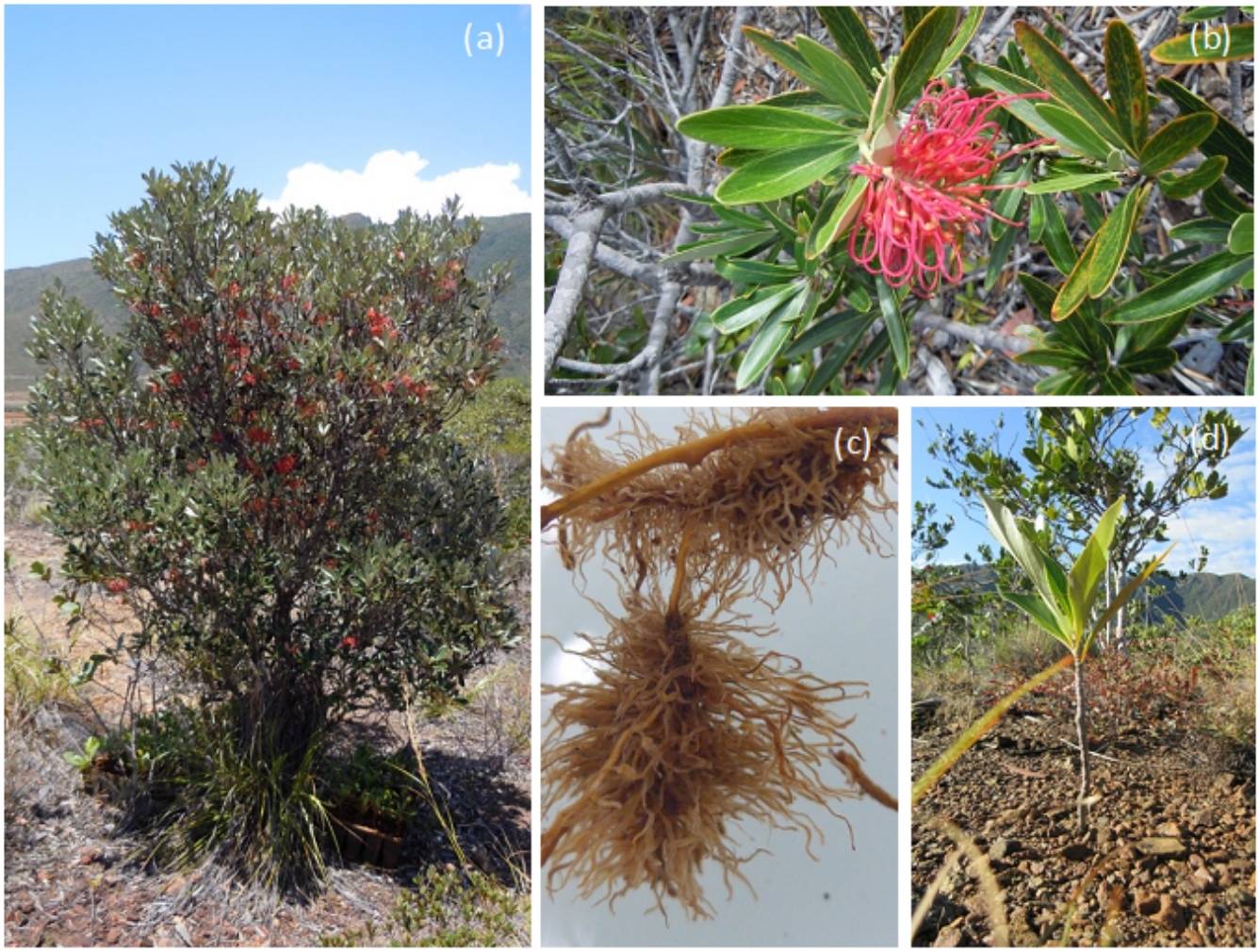

Figure 1

(a) Mature specimen of Grevillea meisneri; (b) Close-up of the inflorescence and the leaves of G. meisneri; (c) Close-up of the cluster roots of G. meisneri; (d) One of the young specimens of G. meisneri used for this study.

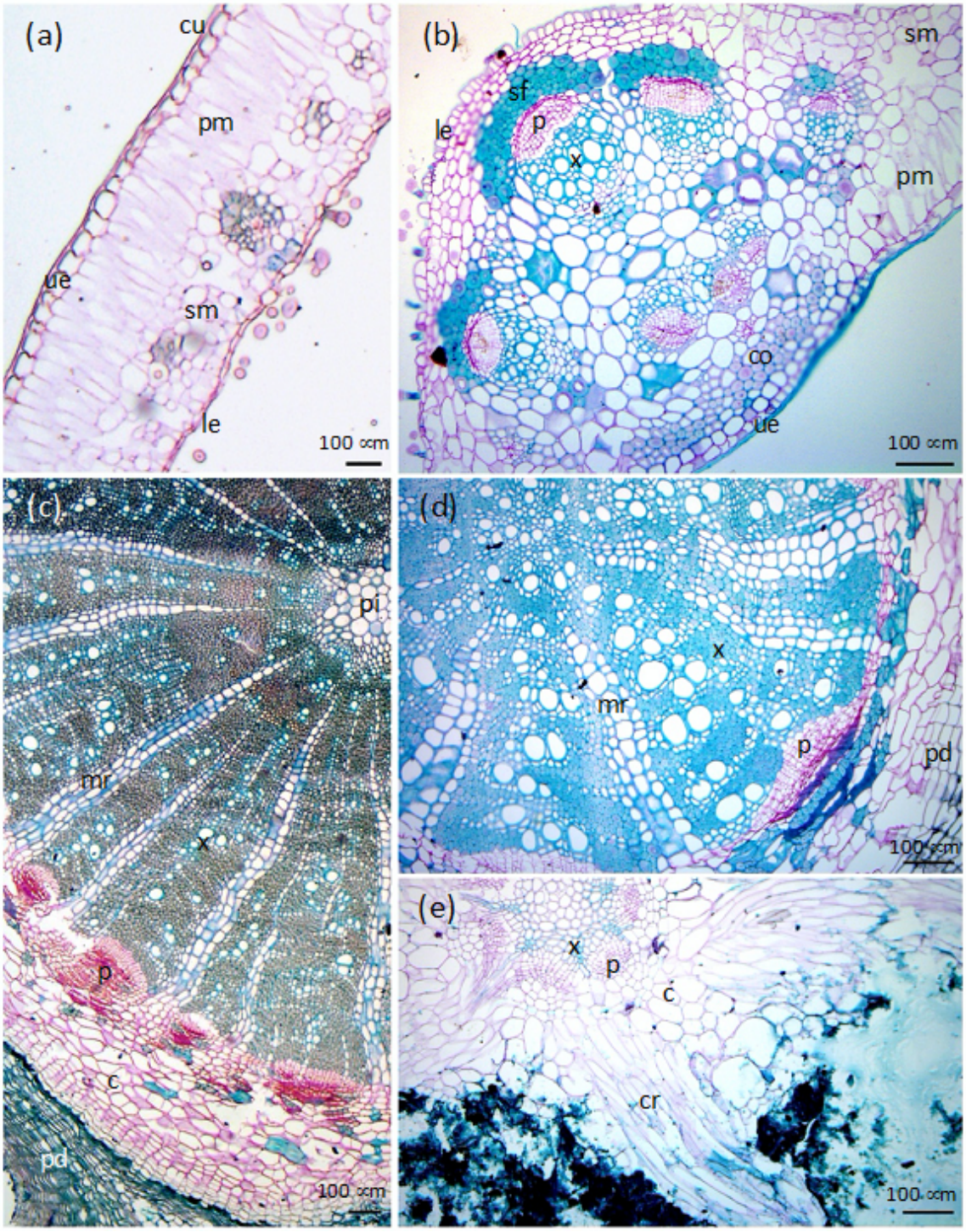

Figure 2

Light microscopy images of Grevillea meisneri anatomical structures. (a) margin of a leaf; (b) mid-rib of a leaf; (c) stem; (d) primary root; (e) secondary root surrounded by the rootlets of a cluster. c, cortex; co, collenchyma; cr, cluster rootlet; cu, cuticle; le, lower epidermis; mr, medullary ray; p, phloem; pi, pith; pm, palisade mesophyll; pd, periderm; sf, sclerenchyma fiber; sm, spongy mesophyll; ue, upper epidermis; x, xylem.

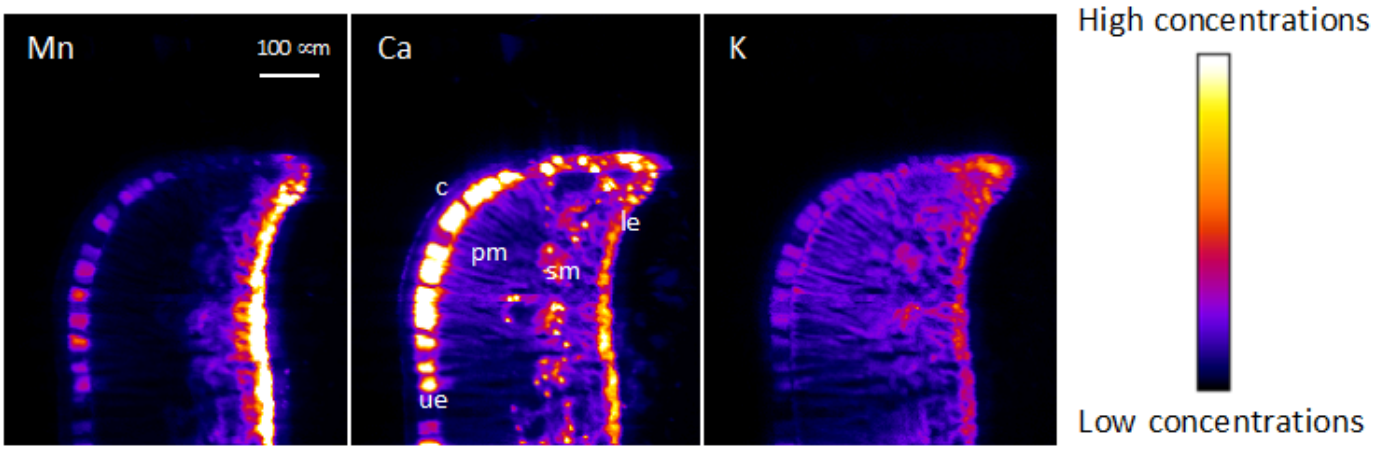

Figure 3

Mn, Ca, and K μXRF maps of a frozen hydrated leaf margin cross section of Grevillea. meisneri. The pixel size is 3 μm. The intensity scales are different between elements. c, cuticle; le, lower epidermis; pm, palisade mesophyll; sm, spongy mesophyll, ue, upper mesophyll.

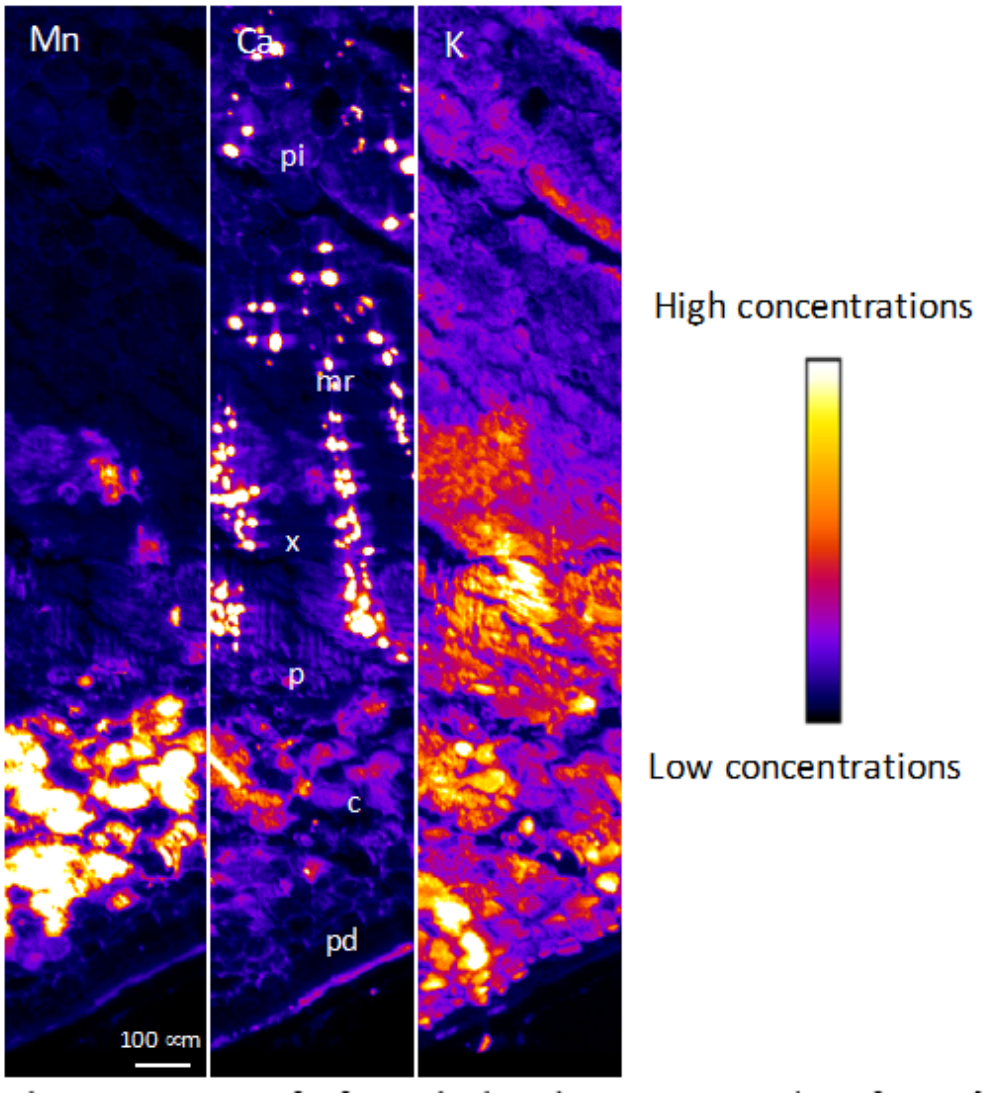

Figure 4

Mn, Ca, and K μXRF maps of a frozen hydrated stem cross section of Grevillea meisneri. The pixel size is 3 μm. The intensity scales are different between elements. c, cortex; mr, medullary ray; p, phloem; pi, pith; pd, periderm; x, xylem.

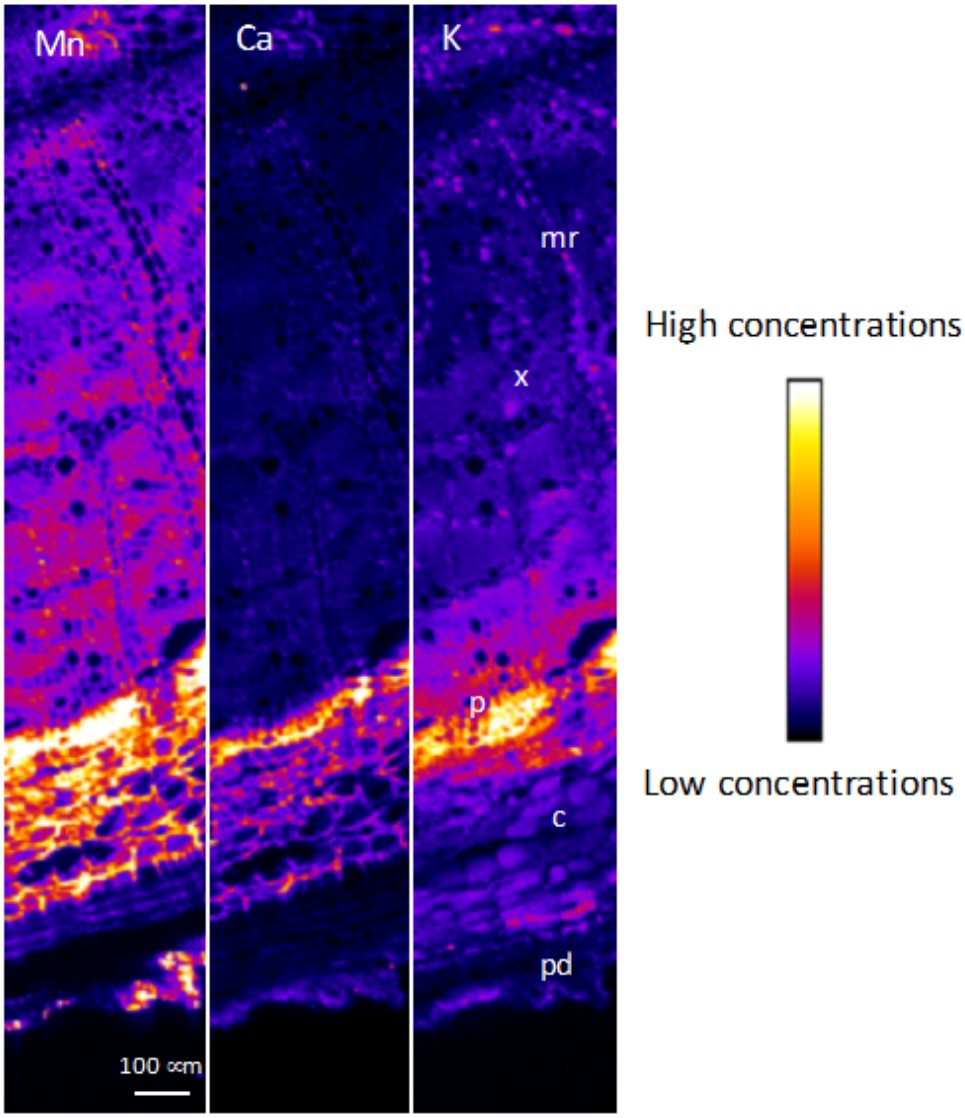

Figure 5

Mn, Ca, and K μXRF maps of a frozen hydrated primary root cross section of Grevillea meisneri. The pixel size is 3 μm. The intensity scales are different between elements. c, cortex; mr, medullary ray; p, phloem; pd, periderm; x, xylem.

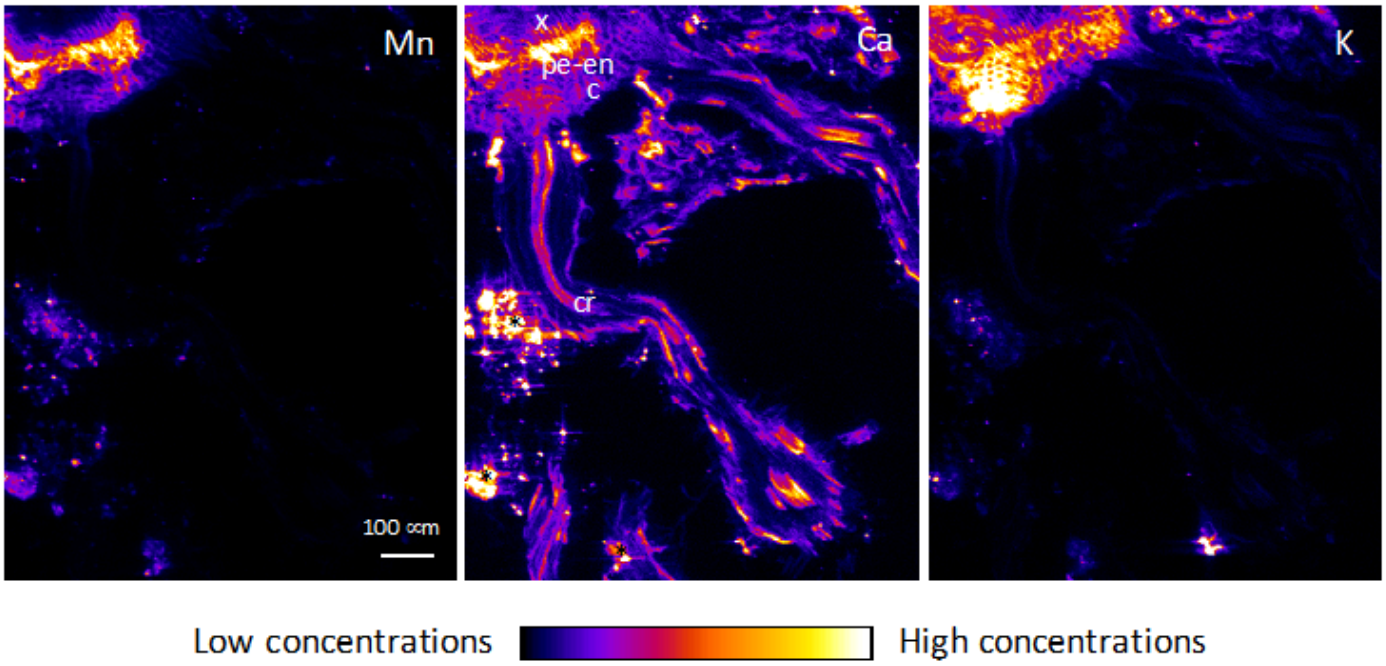

Figure 6

Mn, Ca and K µXRF maps of a frozen hydrated cluster root cross section of Grevillea meisneri. The pixel size is 3 µm. The intensity scales are different between elements. c, cortex; cr, cluster rootlet; p, phloem; pe-en, pericycle-endodermis; x, xylem. Asterisks indicate soil particles.

Supplementary Files

This is a list of supplementary files associated with this preprint. Click to download.

- SIV6FiguresTables.docx